Published in Contributions to Mineralogy and Petrology, 143, issue 2, 192 - 208, 2002
which should be used for any reference to this work


R. Abart · N. Badertscher · M. Burkhard · E. Povoden

# Oxygen, carbon and strontium isotope systematics in two profiles across the Glarus thrust: implications for fluid flow

Received: 28 April 2001 / Accepted: 15 October 2001 / Published online: 23 March 2002

**Abstract** The Glarus thrust is a prominent tectonic feature in the eastern Helvetic Alps. It has been recognized as a potential major pathway for syntectonic crustal scale fluid flow. The oxygen, carbon and strontium isotope patterns obtained from two vertical profiles across the thrust indicate fundamentally different flow regimes in the southern section of the thrust, where the footwall is represented by Mesozoic limestones, and in the northern section, where the footwall is represented by Tertiary flysch. At the Grauberg locality in the south, the observed isotope patterns give evidence of a net mass transport component from the hanging wall Verrucano to the footwall limestone with a maximum time-integrated volumetric fluid flux of 6.1 $m^3/m^2$. In the south, the hydration of the lowermost 10 to 20 m of the hanging wall Verrucano requires introduction of an aqueous fluid by subhorizontal flow along the thrust with a minimum time integrated flux of 240 $m^3/m^2$. At the Lochseite locality in the north, the isotope patterns indicate a vertical mass transport component from the footwall flysch to the hanging wall Verrucano with a time-integrated fluid flux of 2.6 $m^3/m^2$. In the north, the fluids were probably derived from compaction and dehydration of the footwall flysch during thrusting. The ascending fluids were ponded below the Verrucano and 'lubricated' the thrust. Short-term pressure drops associated with seismic motion along the thrust led to the precipitation of calcite in veins at the thrust surface contributing material to the Lochseiten calc-mylonite, a thin calc-mylonite layer at the thrust contact. Although cross thrust fluid flow may have been two to three orders of magnitude smaller than flow along the thrust, it had a major impact on the isotopic composition of the Lochseiten calc-mylonite. In particular, it buffered the oxygen isotope composition of the calc-mylonite towards the relatively $^{18}O$-depleted composition of the hanging wall Verrucano in the south and towards the relatively $^{18}O$-enriched compositions of the footwall flysch in the north. By this mechanism a regional south to north $^{18}O$-enrichment trend was simulated within the Lochseiten calc-mylonite.

R. Abart (✉) · E. Povoden
Institut of Mineralogy and Petrology,
Karl-Franzens-Universitat Graz,
8010 Graz, Austria
E-mail: rainer.abart@unibas.ch
Tel.: +41-61-2673616
Fax: +41-61-2672881

N. Badertscher · M. Burkhard
Institut de Geologie, 2007 Neuchatel, Switzerland

*Present address*: R. Abart
Mineralogisch-Petrographisches Institut,
Universitat Basel, 4056 Basel, Switzerland

## Introduction

Tectonic structures, such as thrusts and faults, are potential pathways for fluid flow (e.g. Fyfe et al. 1978; Fyfe and Kerrich 1985; Oliver 1986; McCaig 1989), and faults and shear zones may channelize fluid flow because of permeability enhancement during deformation (e.g. Etheridge et al. 1984; Cox et al. 1986; Sibson 1986). The stable isotopes of oxygen and carbon as well as strontium isotopes are particularly useful tracers for fluid flow (e.g. Nabelek 1991). In this context, isotopic fronts are of special interest (e.g. Bickle and McKenzie 1987, Baumgartner and Rumble 1988).

Initially, sharp fronts that may exist at lithological contacts may be degraded by diffusive/dispersive[1] processes in the pore fluid and they may be displaced by fluid advection[2]. The geometry of an isotopic front reflects the extent, the mechanisms and the relative rates of

[1]In this context the term dispersion refers to the combined effects of molecular diffusion and hydrodynamic dispersion.

[2]Material transport by solid-state diffusion is several orders of magnitude slower than fluid-bound transport, and will be disregarded in this paper.

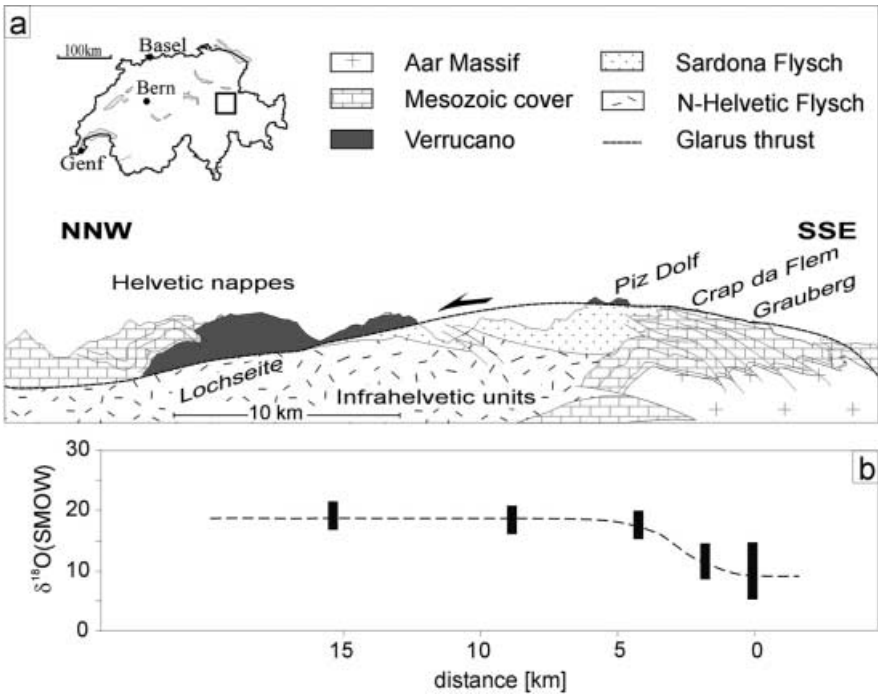


**Fig. 1a.** Simplified cross section of the Glarus thrust, modified from Badertscher et al. (2002); **b** regional south to north $^{18}O$-enrichment trend of calcites from the Lochseiten calc-mylonite as documented by Burkhard and Kerrich (1990). The *dashed line* schematically illustrates the model interpretation of Bowman et al. (1994) as an oxygen isotope front produced by combined northward-directed thrust parallel flow and diffusion/dispersion in the pore fluid

the processes involved in mass transport and mineral–fluid exchange (e.g. Abart and Pozzorini 2000).

The Glarus thrust is a very well-defined major thrust-fault structure in the eastern Helvetic Alps. A schematic cross section of the thrust is given in Fig. 1a. Permian siltstones and shales of the Verrucano formation were thrust over Mesozoic limestones in the south and Tertiary Flysch in the north during Early Miocene times. The thrust surface is characterized by the presence of a thin (< 1 to 5 m thick) continuous layer of calc-mylonite, which will be referred to here as the 'Lochseiten calc-mylonite' (the 'Lochseiten limestone' of Heim 1921)[3]. Burkhard and Kerrich (1990) and more recently Badertscher et al. (2002) documented a regional south to north trend of $^{18}O$ enrichment in the Lochseiten calc-mylonite (see Fig. 1b). This trend was interpreted by Burkhard et al. (1992) and Bowman et al. (1994) as an oxygen isotope front produced by northward migration of $^{18}O$ depleted fluids along the thrust. Based on the oxygen isotope compositions of the Lochseiten calc-mylonite and using a strictly one-dimensional model Bowman et al. (1994) derived time-integrated volumetric fluid fluxes on the order of 5,000 $m^3/m^2$ for flow along the thrust and characterized the transport mechanisms for the inferred crustal scale flow system. The latter authors did not take into account the possible interactions of the Lochseiten calc-mylonite with the footwall and hanging wall lithologies. Such interactions are, however, likely because the vertical extent of the Lochseiten calc-mylonite is vanishingly small compared with its horizontal extent. At the thrust contact, lithologies with strongly contrasting isotopic compositions were juxtaposed and are separated only by the thin Lochseiten calc-mylonite layer. In this geological context, the isotope composition of the calc-mylonite may well have been influenced by material transport in the direction perpendicular to the thrust as well as by fluid migration along the thrust; we here investigate such cross thrust transport components. We present petrographic as well as oxygen, carbon and strontium isotope data from two vertical profiles at the Grauberg and the Lochseite localities, respectively. These are among the southernmost (Grauberg) and northernmost (Lochseite) exposures of the thrust. In particular, we investigate the possible influence of cross thrust isotopic exchange on the isotopic composition of the Lochseiten calc-mylonite. This information is crucial for the interpretation of regional south to north oxygen isotope trends reported from the Lochseiten calc-mylonite by Burkhard and Kerrich (1990) and by Badertscher et al. (2002).

[3]In this communication, the term Lochseiten calc-mylonite is only used for calc-mylonite with abundant macroscopically distinguishable veins. Grey calc-mylonites, which were unambiguously derived from the footwall limestones in the southern section of the thrust, are not included in this definition.

## Geologic setting

### Regional geology

The Glarus thrust is a major tectonic feature in the Helvetic Alps of eastern Switzerland (see Fig. 1a). It separates the Helvetic nappes in the hanging wall of the thrust from the Infrahelvetic units in the footwall. The Helvetic nappes are a series of thin skinned décollement nappes comprised of Permian to Eocene sediments. The Infrahelvetic units comprise a crystalline basement with

its para-autochthonous Mesozoic to Tertiary sedimentary cover and also include allochthonous slices of south-Helvetic (Blattengrat) and Penninic (Sardona) flysch. The latter units have been emplaced on the para-autochthonous units (N-Helvetic flysch) during an Oligocene deformation phase, referred to as the Pizol phase (Pfiffner 1977). The whole Infrahelvetic complex was penetratively folded during the Upper Oligocene Calanda phase. The thrusting event, referred to as the Ruchi phase occurred during the Early Miocene (Milnes and Pfiffner 1980) and represents the youngest major deformation event in the eastern Helvetic Alps.

The Glarus thrust is exposed as an exceptionally sharp horizon over an area of about 600 $km^2$. The hanging wall is generally represented by the Verrucano formation, a clastic series of predominantly siltstones and shales with minor intercalations of conglomerates and volcanoclastic horizons. In the southernmost exposures, Verrucano is thrust over para-autochthonous Late Jurassic to Early Cretaceous limestones. In the north, the footwall of the thrust is represented by an up to 2-km-thick sequence of N-Helvetic flysch primarily comprised of marly slates, sandstones and conglomerates. North of the Lochseiten locality, the Glarus thrust plunges below topography. It is interpreted to merge with the basal Helvetic Säntis thrust (Schmid et al. 1996) where higher Helvetic nappes are thrust over Late Oligocene to Early Miocene Molasse. Balanced cross sections indicate that the Glarus thrust extends to mid-crustal levels some 20 km south of the southernmost exposures (Pfiffner 1985). It may be rooted behind either one of the Aare, Tavetsch, and Gotthard crystalline massifs (e.g. Burkhard et al. 1992).

Metamorphic grade ranges from 'anchizonal' (i.e. ≥200 °C) in the north and in the footwall flysch to lower greenschist facies (i.e. ≅350 °C) in the south and in the hanging wall Verrucano.

The anchi/epi zone boundary is offset along the Glarus thrust by about 2 km because of post-metamorphic thrusting (Rahn et al. 1995), and an inverse metamorphic gradient is documented across the thrust contact (Frey 1988). The Glarus thrust probably developed at a crustal depth of 10 to 15 km, corresponding to lithostatic pressures of about 300 to 450 MPa. Metamorphism in the hanging wall Verrucano was dated by Hunziker et al. (1986) and Hunziker (1987) at 30 Ma. Concordant K/Ar and Rb/Sr ages of illite ( < 2 μm) from the Lochseite locality indicate that thrusting was active till at least 23 Ma.

## The thrust contact at Grauberg

The Grauberg section is located about 2 km northwest of Segnashütte (Swiss co-ordinates 736.250/192.700) at an elevation of 2,300 m above sea level. There, about 5 m of vertical section of footwall limestone, a 25-cm-thick layer of Lochseiten calc-mylonite and over 100 m of vertical section of the hanging wall Verrucano are exposed. The footwall consists of Upper Jurassic to Lower Cretaceous massive grey limestones comprised of calcite ( > 95 vol% ) and minor amounts of quartz and muscovite. A pronounced foliation, dipping about 30 to 40°SSE, is ascribed to the pre-thrusting Calanda phase (Milnes and Pfiffner 1980). In the uppermost metre below the thrust contact, this foliation is progressively rotated parallel to the thrust. Within this shear zone, the limestones are transformed to grey calc-mylonites with a planar millimetre-scale banding defined by the alternation of pure carbonate layers with more mica rich layers and by layer parallel calcite veins (see Fig. 2a). Within the mica rich layers dolomite occurs as a second carbonate phase. The $H_2O$ and $CO_2$ contents of selected samples are shown in Fig. 3. The $CO_2$ content systematically decreases from close to 44 to about 41 wt% within the uppermost 2 meters of the footwall limestones. At the same time, the water content increases from about 0.15 to 0.4 wt%.

A 25-cm-thick yellowish calc-mylonite layer sandwiched between the grey footwall limestones and the hanging wall Verrucano represents the Lochseiten calc-mylonite. It shows a planar mylonitic banding defined by an alternation of calcite veins, a fine grained calcite matrix and stylolites comprised of muscovite. In the matrix, the grain size is generally less than 5 μm, and within veins the calcites may be up to 100 μm in diameter. The $CO_2$ content of the calc-mylonite is between 38 and 41 wt% (see Fig. 3), testifying to the presence of a significant fraction of silicate phases. The contact with the Verrucano is sharp.

The hanging wall Verrucano is primarily comprised of quartz, albite, muscovite, chlorite and calcite. It has a mylonitic texture, where layers rich in albite and quartz alternate with muscovite–chlorite-rich layers. It shows an intense thrust parallel foliation with frequent northward-dipping shear bands indicating thrusting with top to the north. The bulk of the quartz–albite matrix is recrystallized at a grain size of generally less than 50 μm. At distances of more than 2 m above the thrust, quartz and albite occasionally occur as up to 1-mm-sized clasts. The bulk rock water content progressively increases from about 2 wt% at 20 m above the thrust to 4.5 wt% at the calc-mylonite/Verrucano contact (see Fig. 3). The hanging wall Verrucano has a 'background' carbonate content of about 5 to 10 wt% $CaCO_3$-equivalent. In the lowermost 10 cm of the Verrucano, the carbonate content is significantly elevated to about 20 wt% $CaCO_3$-equivalent (see Fig. 3). Calcite usually occurs as late phase in fracture fillings. Locally ankerite is found as a second carbonate phase. It occurs as well-crystallized idiomorphic grains in textural equilibrium with the mylonitic quartz–albite matrix. At distances of more than 2 m above the thrust, haematite and ilmenite are the dominating opaque phases. Towards the thrust, ilmenite is replaced by titanite and the main opaque phase is pyrite.

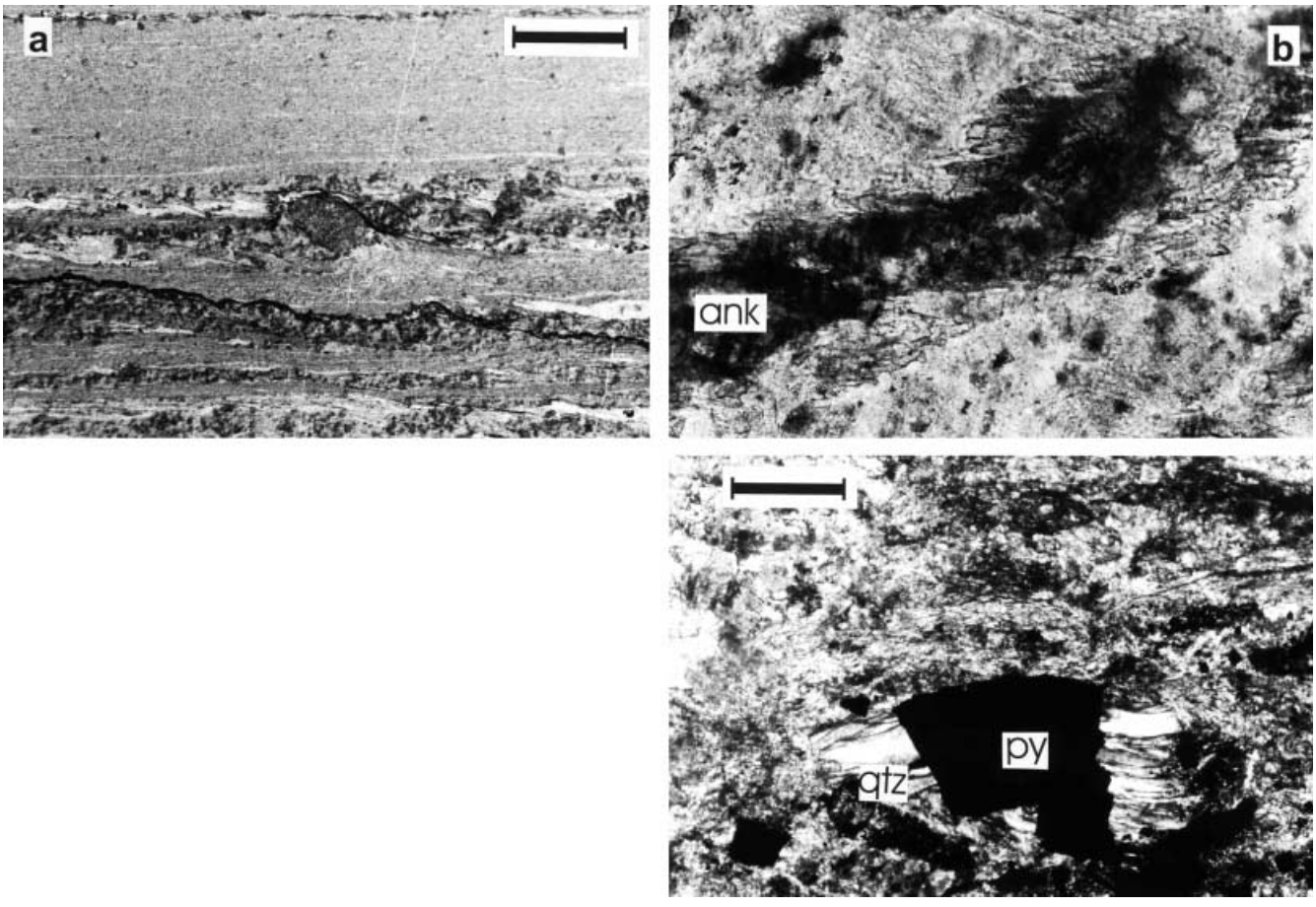


**Fig. 2a.** Footwall limestone from 65 cm below the thrust contact at Grauberg (sample G029), pure carbonate layers alternate with more mica rich domains on a millimetre scale, the mica rich parts represent low $^{18}O$ domains and contain abundant rotated dolomite blasts, *scale bar* 500 μm; **b** hanging wall Verrucano from 30 cm above the thrust contact at Lochseite (sample LS03), microscopic fracture filled with ankerite (*dark*) and fibrous quartz, *scale bar* 50 μm; **c** hanging wall Verrucano from 10 cm above the thrust contact at Lochseite (sample LS01), fibrous quartz in pressure fringes around pyrite, crossed polars, *scale bar* 500 μm

## The thrust contact at Lochseite

The Lochseiten locality is situated some 2 km east of the village of Schwanden, at Swiss coordinates 725.860/206.400 at an elevation of 600 m a.s.l. There a vertical section of about 1 m of footwall flysch, a ~50-cm-thick layer of Lochseiten calc-mylonite and a 20-m vertical section of the hanging wall Verrucano are exposed.

The footwall flysch is comprised of marly slates with shale layers alternating with impure sandstone layers at millimetre scale. The common mineral assemblage is illite–chlorite–albite–quartz–calcite–organic material. Close to the strongly lobate-cuspate contact with the calc-mylonite the flysch is intensively folded and has a chaotic structure. Further down it shows a more regular slaty cleavage.

The ~50-cm-thick layer of Lochseiten calc-mylonite is characterized by a high density of millimetre-thick veins, which are intensely folded, refolded and disrupted. They give a turbulent appearance to the rock referred to as a knead structure by Heim (1921). A planar, thrust parallel brittle structure referred to as the septum crosscuts all internal structures. This feature has been interpreted as a cataclasite that formed during the last stages of thrusting (e.g. Funk et al. 1983).

The hanging wall Verrucano is comprised of massive siltstone and conglomerate horizons alternating with subordinate shale layers.

The main constituents of Verrucano are quartz, albite, muscovite, calcite and chlorite. In the lowermost 1–2 m above the thrust, the Verrucano is partially mylonitized and has a green colour. Further away from the thrust, the mylonitic foliation dies out and the rock obtains a reddish colour, which is characteristic of unaltered Verrucano from the northern section of the Glarus Alps.

Quartz and albite clasts are up to 5 mm at distances of more than 10 m above the calc-mylonite/Verrucano contact. Towards the thrust, they are progressively transformed into fine-grained quartz–albite aggregates, and albite clasts show progressive alteration to sericite. The bulk-rock water content increases from about 2.5 wt% at 8 m above the thrust to 4 wt% at the calc-mylonite/Verrucano contact (see Fig. 3). In the lowermost 2 m above the thrust, abundant fractures in quartz and albite clasts are sealed with newly formed fibrous

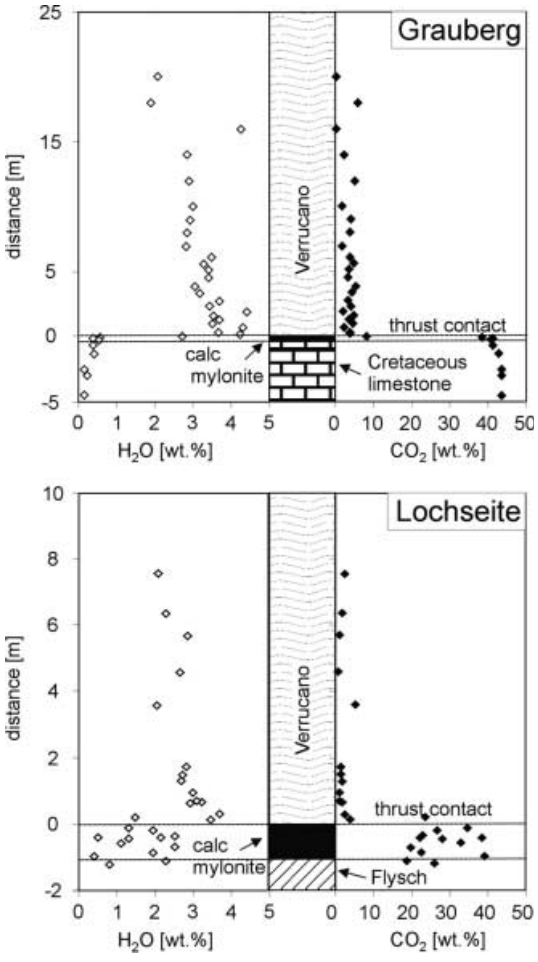


**Fig. 3.** Bulk rock $H_2O$ and $CO_2$ contents of selected samples from sampling profiles across the Glarus thrust at the Grauberg and Lochseite localities

quartz, ankerite and calcite (see Fig. 2b). Newly formed quartz is also observed in pressure fringes around pyrite (see Fig. 2c). At distances of more than 2 m above the thrust, albite and quartz occur at about equal proportions. In the lowermost 2 m above the thrust, albite is significantly less abundant than quartz with molar albite to quartz ratios of generally less than 0.15. As in the Grauberg rocks, calcite occurs as the prime carbonate phase in cracks and fissures.

The background carbonate content is, however, only 1 to 5 wt% $CaCO_3$-equivalent (see Fig. 3). At the contact to the thrust, the carbonate content increases to about 10 wt% $CaCO_3$-equivalent.

## Sampling and analytical methods

### Sampling

Profiles across the Glarus thrust were sampled at Grauberg and the Lochseite localities. At Grauberg, samples were taken with a rock saw to ensure recovery of unweathered material.

At the Lochseiten locality, samples were taken with the permission of the Direktion für Landwirtschaft, Wald und Umwelt of the Kanton of Glarus. Because of natural heritage regulations, samples could only be taken with a hammer. Samples were taken at decimetre intervals in the first metre below and above the thrust contact, and at metre intervals further away. An aliquot of 40 g of each sample was crushed in a jaw crusher and ground to a powder with a grain size of $< 40$ μm in a tungsten carbide mill. Rock powders were used for bulk rock analyses and for mineral separation.

### Stable isotope analyses

For stable isotope analysis of carbonates, bulk rock powders with an equivalent 0.1–0.3 mg carbonate content were loaded into individual glass vials. $CO_2$ was extracted by reaction with 102% $H_3PO_4$ at 70 °C for 4 min on a Finnigan Kiel II device. The $CO_2$ was analysed on line with a Finnigan-MAT Delta$^{plus}$ isotope ratio mass spectrometer. Reproducibility of replicate measurements was better than 0.1‰ ($1\sigma$) for both $\delta^{18}O$ and $\delta^{13}C$. In addition to bulk rock samples we analysed carbonate microsamples taken with a dentist drill from polished rock surfaces.

Quartz–albite separates were obtained from the Verrucano samples by means of chemical purification techniques (Kiely and Jackson 1964; Syers et al. 1968). For the analysis of quartz, about 2 mg of quartz–albite concentrate were loaded into a nickel sample holder. Albite was removed quantitatively by fluorination in a $BrF_5$ atmosphere for 12 h at room temperature. The purity of the remaining quartz was routinely checked by XRD analysis. To test for the possible influence of the purification procedure on the oxygen isotope composition of quartz, two standard quartz samples were run through an identical procedure as the samples. Oxygen isotope analysis showed no significant alteration of the $\delta^{18}O$ values of quartz. As albite could not be separated from quartz, its oxygen isotope composition was determined from the oxygen isotope composition of quartz–albite mixtures with known albite/quartz ratios and known oxygen isotope composition of quartz. To minimize the loss of albite, pre-fluorination was done for 9 min only. The quartz/albite proportions of the samples after pre-fluorination were determined by XRD.

Oxygen was extracted from mineral separates on a laser fluorination line as described by Sharp (1990). Samples of 1–2 mg were reacted in a $BrF_5$ atmosphere under a slightly defocused 25 W $CO_2$ laser beam. The liberated oxygen was separated from excess reagent and reaction by-products cryogenically and by means of a 20-cm KBr column kept at 120 °C. $O_2$ was collected on a molecular sieve at liquid nitrogen temperatures and finally expanded into the variable volumes of a Finnigan Delta$^{plus}$ isotope ratio mass spectrometer. UWG-2 garnet (Valley et al. 1995) was used as an internal standard. Reproducibility of replicate measurements was better than 0.15‰ ($1\sigma$). Oxygen isotope compositions are given in the conventional $\delta$-notation relative to V-SMOW.

### Strontium isotope analyses

The $^{87}Sr/^{86}Sr$ ratios of the carbonate fraction of 20 selected samples were analysed. The mechanical separation of the carbonate and silicate fraction was impossible. To minimize contamination of the carbonate-derived strontium by silicate-derived strontium, granulates with a grain size of 500 μm were used for acid leaching. The granulates were initially treated with 2.5 M HCl at room temperature. Strontium was isolated using a standard ion exchange technique. The $^{87}Sr/^{86}Sr$ ratios were normalized to NBS-987 = 0.71022. Analytical precision was better than 0.000011 ($2\sigma$).

Because of the young age of the tectonic activity along the Glarus thrust (Hunziker et al. 1986), age corrections for radiogenic strontium are negligible (Burkhard et al. 1992).

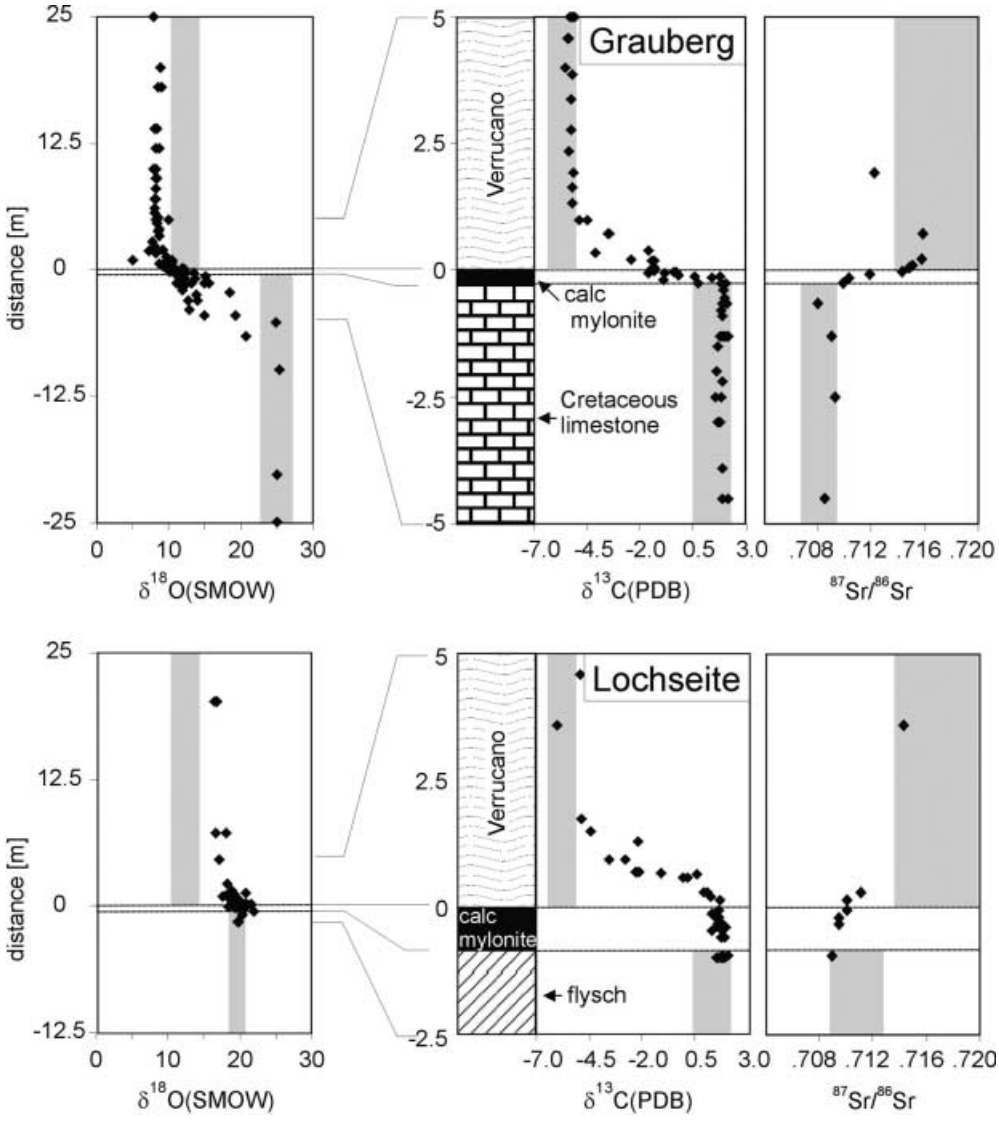


**Fig. 4.** Oxygen, carbon and strontium isotope compositions of calcite from the two sampling profiles across the thrust contact at the Grauberg and Lochseite localities, *grey bars* indicate isotopic compositions of corresponding unaltered reference lithologies

Determination of water and carbonate contents

$H_2O$ and $CO_2$ contents were determined on a Leco RC-412 elemental analyser. The samples were roasted at 1,000 °C under excess oxygen. The $H_2O$ and $CO_2$ gases produced were monitored simultaneously on infrared cells. Reproducibility of measurements was better than 0.04 wt% ($1\sigma$) for both $H_2O$ and $CO_2$.

## Stable isotope data

### $^{18}O$ and $^{13}C$ variations across the thrust

The oxygen and carbon isotope compositions of carbonates from the two sampling profiles across the thrust contact at the Grauberg and Lochseite localities are shown in Fig. 4. At the Grauberg locality, a smooth transition from relatively $^{18}O$ enriched compositions with $^{18}O$ values of about 25‰ relative to SMOW in the footwall carbonates to relatively $^{18}O$ depleted compositions of about 8.5‰ in the hanging wall Verrucano was observed. At Lochseite, a similarly smooth transition from about 20‰ in the footwall flysch to 17‰ in the hanging wall Verrucano is documented.

There are two fundamental differences between the oxygen isotope profiles of Lochseite and Grauberg. First, the oxygen isotope compositions of the footwall grey limestones of Grauberg are systematically depleted, beginning at about 5 m below the thrust. In contrast, the uppermost flysch carbonate samples at Lochseite do not show any oxygen isotope alteration.

Their $\delta^{18}O$ values are similar to the $\delta^{18}O$ values of carbonate from the unaltered flysch (18.5–20.5‰ according to Burkhard and Kerrich 1990; Badertscher et al. 2002). Second, above the thrust contact at Grauberg, the oxygen isotope compositions of calcite in Verrucano level out at about 8.5‰ at a distance of 2.5 m from the thrust. In contrast, at Lochseite, the corresponding $^{18}O$ values gradually decrease from about 20‰ at the calc-mylonite/Verrucano contact to 17‰ at 20 m above the thrust. The 'background' composition of

carbonates from the Verrucano is about 13‰ as determined in samples from about 100 m above the thrust (Badertscher et al. 2002). This composition is not attained in the lowermost 20 m above the thrust.

The carbon isotope compositions are $\delta^{13}C(PDB) \approx 2‰$ in unaltered footwall rocks of both the Grauberg and Lochseite localities. At Grauberg, a steep systematic depletion trend from $\delta^{13}C \approx 2‰$ at 25 cm below the calc-mylonite/Verrucano contact to $\delta^{13}C \approx -0.9‰$ at the contact is observed within the calc-mylonite. In the hanging wall Verrucano, this trend flattens and declines, and the $\delta^{13}C$ values level out at a composition of about –5‰ at about 1.5 m above the thrust contact. At Lochseite, a $^{13}C$ depletion trend is only observed within the Verrucano, where $\delta^{13}C$ values decrease from about 2‰ at the calc-mylonite/Verrucano contact to a 'background' composition of –6‰ 2 m above the thrust.

## Small-scale $\delta^{18}O$ variations in the footwall limestones at Grauberg

The oxygen isotope compositions of the footwall limestone at Grauberg are shown in Fig. 5. Whereas the bulk carbonate samples define a relatively smooth $^{18}O$ trend, the oxygen isotope compositions of microsamples taken from veins and matrix may vary considerably at small scale. The veins may be both depleted or enriched in $^{18}O$ relative to the bulk sample carbonate by up to 2‰. Small-scale oxygen isotope heterogeneities may be even more pronounced within the fine grained matrix. Relatively $^{18}O$-enriched parallel domains with $\delta^{18}O$ of 21–23‰ alternate at the millimetre scale with more depleted domains, where $\delta^{18}O$ is between 11 and 13‰ (see Fig. 5). Oxygen isotope gradients of about 10‰ are documented over distances as small as 2 mm. The isotopically relatively 'heavy' domains correspond to pure calcite layers. The relatively $^{18}O$-depleted domains coincide with layers that contain abundant micas and dolomite grains.

## Quartz–calcite oxygen isotope systematics

The oxygen isotope compositions of quartz, albite and calcite and the corresponding inter-mineral fractionations from the sampling profiles at Grauberg and Lochseite are shown in Fig. 6. At Grauberg, quartz shows a subtle trend of $^{18}O$ enrichment from about 11.5‰ at more than 10 m above the thrust to about 13.5‰ at the calc-mylonite/Verrucano contact. The concomitant $^{18}O$ enrichment in calcite is more pronounced, especially within the lowermost 50 cm of the Verrucano (see Fig. 6). As a consequence, the quartz–calcite fractionations decrease from about 4‰ at 2.5 m above the thrust to less than 2‰ at the calc-mylonite/Verrucano contact.

At Lochseite, quartz shows a pronounced trend of $^{18}O$ enrichment from about 15‰ at 8 m above the thrust, to about 23‰ at the calc-mylonite/Verrucano contact (see Fig. 6). Albite shows a similar trend, which is less well established because of the absence of albite in the lowermost 0.5 m above the thrust. The concomitant $^{18}O$ enrichment in calcite is less pronounced, and the quartz–calcite fractionations increase from about –2.5‰ at more than 2 m above the thrust to 3.5‰ at the calc-mylonite/Verrucano contact (Fig. 6).

## Strontium isotope data

The $^{87}Sr/^{86}Sr$ ratios of calcite analysed in selected samples from the two vertical profiles at the Grauberg and

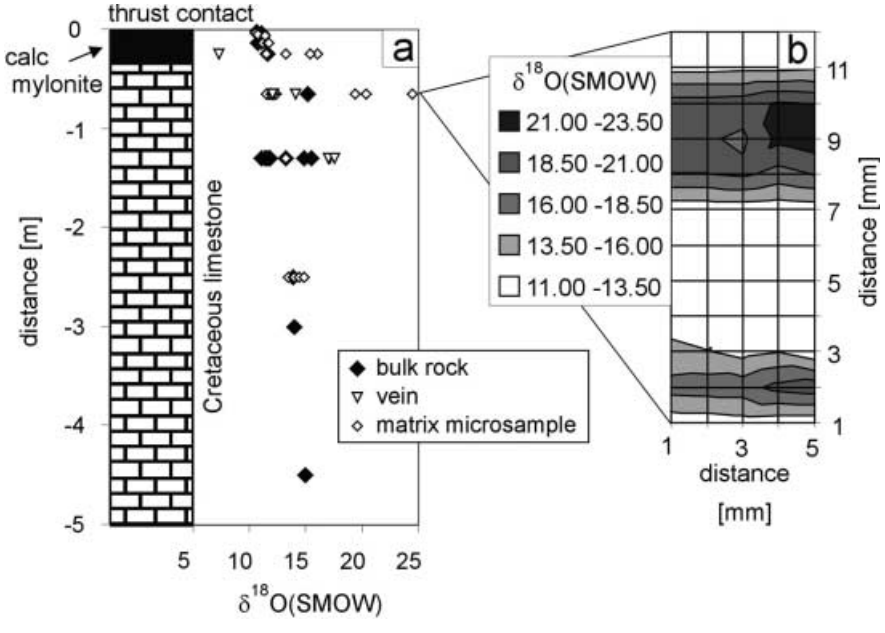


**Fig. 5a.** Oxygen isotope compositions of calcite from a sampling profile through the Lochseiten calc-mylonite and the footwall limestone at Grauberg; **b** small-scale oxygen isotope variations in a polished slab from the footwall limestone taken at 65 cm below the thrust contact (sample G029); 60 microsamples were taken with a dentist drill from a polished rock surface, sampling positions approximately coincide with the grid intersection points

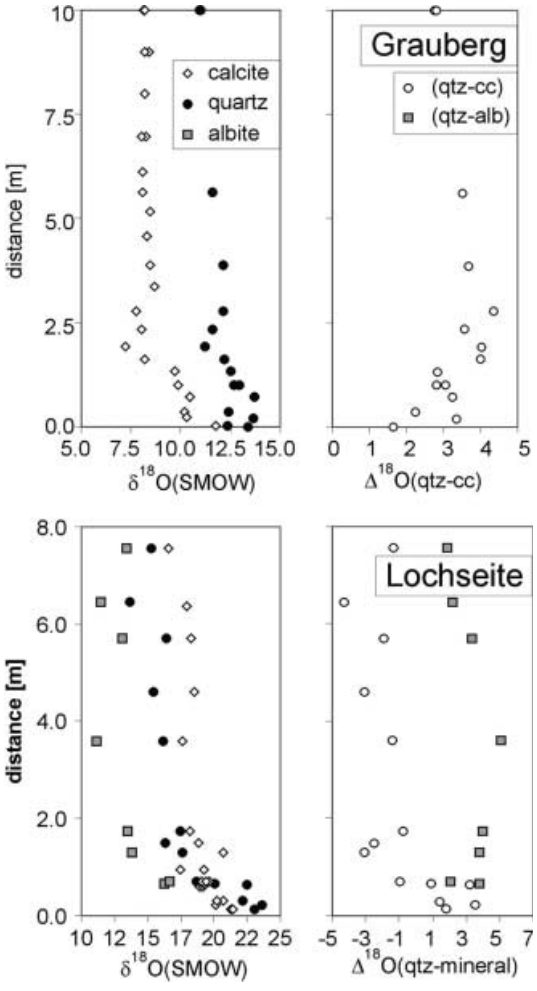


**Fig. 6.** Oxygen isotope compositions of calcite and coexisting quartz (and albite) and corresponding inter-mineral oxygen isotope fractionations from the hanging wall Verrucano at the Grauberg and Lochseite localities

the Lochseite localities are shown in Fig. 4. At Grauberg, the $^{87}Sr/^{86}Sr$ values range from 0.708 in the footwall limestones to 0.716 in the hanging wall Verrucano with a smooth transition in a narrow zone along the thrust contact. The $^{87}Sr/^{86}Sr$ values of the footwall limestones are well within the range of the strontium isotope ratios typical for marine carbonates of Mesozoic to Early Miocene age (0.707–0.7089 according to DePaolo 1986; Burke et al. 1982). The $^{87}Sr/^{86}Sr$ values of the Verrucano samples are similar to those obtained by Hunziker et al. (1986; 0.7136–0.7211 at 30–20 Ma). The transition between these two strontium reservoirs is confined to a narrow zone ranging from about 25 cm below to about 15 cm above the calc-mylonite/Verrucano contact.

The $^{87}Sr/^{86}Sr$ gradient is steepest within the Lochseiten calc-mylonite where the $^{87}Sr/^{86}Sr$ are 0.710 at the contact with the footwall carbonates and 0.714 at the contact with the Verrucano. A small but readily detectable shift in the $^{87}Sr/^{86}Sr$ values from 0.7148 to 0.7158 is identified in the lowermost 15 cm of the hanging wall Verrucano.

At the Lochseite locality, the $^{87}Sr/^{86}Sr$ values of calcite vary from 0.709 in the footwall flysch to 0.714 in the Verrucano. The flysch values agree well with the range of 0.7089–0.713 given by Hunziker et al. (1986) for the carbonate fraction of low grade metasediments of the Infrahelvetic complex. There is a smooth transition between the Verrucano and flysch strontium reservoirs.

In contrast to the Grauberg profile, at Lochseite most of the strontium isotope variation occurs within the hanging wall Verrucano. Within the Verrucano, the $^{87}Sr/^{86}Sr$ ratios range from 0.710 at the calc-mylonite/Verrucano contact to 0.714 at 3.5 m above the thrust. The Lochseite calc-mylonite shows $^{87}Sr/^{86}Sr$ ratios of 0.710 with only minor internal variation (also compare with Burkhard et al. 1992).

## Discussion

### Mineralogical changes associated with thrusting

In the unaltered Verrucano of both localities, the major minerals are quartz, oligoclase, potassium feldspar, muscovite and chlorite with some biotite and calcite. As the thrust is approached from some 50 m distance, albite, quartz, chlorite and muscovite/illite gradually become the dominant silicate phases and the bulk rock water content increases from ~2 to ~5 wt% (see Fig. 3). This suggests that hydration reactions occurred near the thrust that led to the replacement of oligoclase, potassium feldspar and biotite by albite, quartz, sericite and chlorite. Assuming that aluminium was conserved, the corresponding reactions may be written as:

$$3KAlSi_3O_8 + 12H_2O + 2H^+ = KAl_3Si_3O_{10}(OH)_2 + 2K^+ + 6H_4SiO_4$$
$$3CaAl_2Si_2O_8 + 4H^+ + 2K^+ = 2KAl_3Si_3O_{10}(OH)_2 + 3Ca^{2+}$$
$$2KMg_3AlSi_3O_{10}(OH)_2 + 6H_2O + 4H^+ = Mg_5Al_2Si_3O_{10}(OH)_8 + 3H_4SiO_4 + 2K^+ + Mg^{2+}$$

Newly formed sericite and chlorite are frequently found as fracture fillings and in pressure shadows of rigid objects (also compare with Arkai et al. 1997). The liberated silica was precipitated as quartz, whose syntectonic growth is well documented for the lowermost 2 m of Verrucano by fibrous aggregates in fractures and in pressure fringes (see Fig. 2b, c). At Grauberg, the occurrence of partially syntectonically grown dolomite along stylolites and mica-rich layers in the uppermost metre of the footwall limestone suggests the introduction of magnesium-bearing species that were probably derived from the biotite to chlorite transformation in the hanging wall Verrucano.

The fact that the carbonate content of unaltered Verrucano is relatively constant and does not show any systematic variation with distance from the thrust suggests that this is caused by pre-thrusting diagenetic and metamorphic processes. The occurrence of calcite as fracture fillings indicates that it was remobilized and recrystallized during deformation. Syntectonic calcite

metasomatism in the Verrucano caused by the introduction of Ca- and carbonate-bearing species from the footwall was restricted to the lowermost 10 cm above the thrust (compare also with Burkhard and Kerrich 1990).

In the footwall limestone and in the calc-mylonite material, transfer in the process of ongoing dissolution and precipitation is suggested by abundant stylolites and veins. A net decrease of carbonate content in the uppermost metre towards the thrust contact at Grauberg (Fig. 3) suggests a net carbonate loss in the course of this process.

## Oxygen and carbon isotope profiles across the thrust

The isotopically contrasting footwall and hanging wall lithologies are regarded as two distinct carbon and oxygen reservoirs, which may exchange material by diffusive/dispersive and advective transport in the pore fluid. The oxygen and carbon isotope transitions at both the Grauberg and Lochseite localities are characterized by monotonic enrichment/depletion trends across the thrust and are interpreted as isotopic fronts. The isotopic composition of the calc-mylonite is never outside the range between the compositions of the footwall and hanging wall lithologies in any of the three isotope systems investigated.

The propagation of a reactive tracer isotope in a one-dimensional system, where transport occurs by diffusion/dispersion in the pore fluid and by fluid advection, may be represented by (e.g. Bear 1972):

$$D\frac{\partial R_f}{\partial x^2} - v\frac{\partial R_f}{\partial x} = \frac{\partial R_f}{\partial t} + \sum_{k=1}^{M}\frac{X_k}{X_f}\frac{\partial R_f}{\partial t}, \quad (1)$$

where $R_f$ and $R_k$ are the isotopic compositions of the pore fluid and of mineral $k$; $x$ and $t$ are distance and time; $D$ and $v$ are the effective diffusion/dispersion coefficient of the isotopic species and the mean interstitial particle velocity; and $X_k$ and $X_f$ are the mole fractions of the isotopic element contained in mineral $k$ and in the fluid, respectively.

## Oxygen and carbon isotope fronts at the Lochseite locality

The fact that the footwall flysch does not show any sign of isotopic alteration at the Lochseite locality suggests that upward material transport was particularly efficient

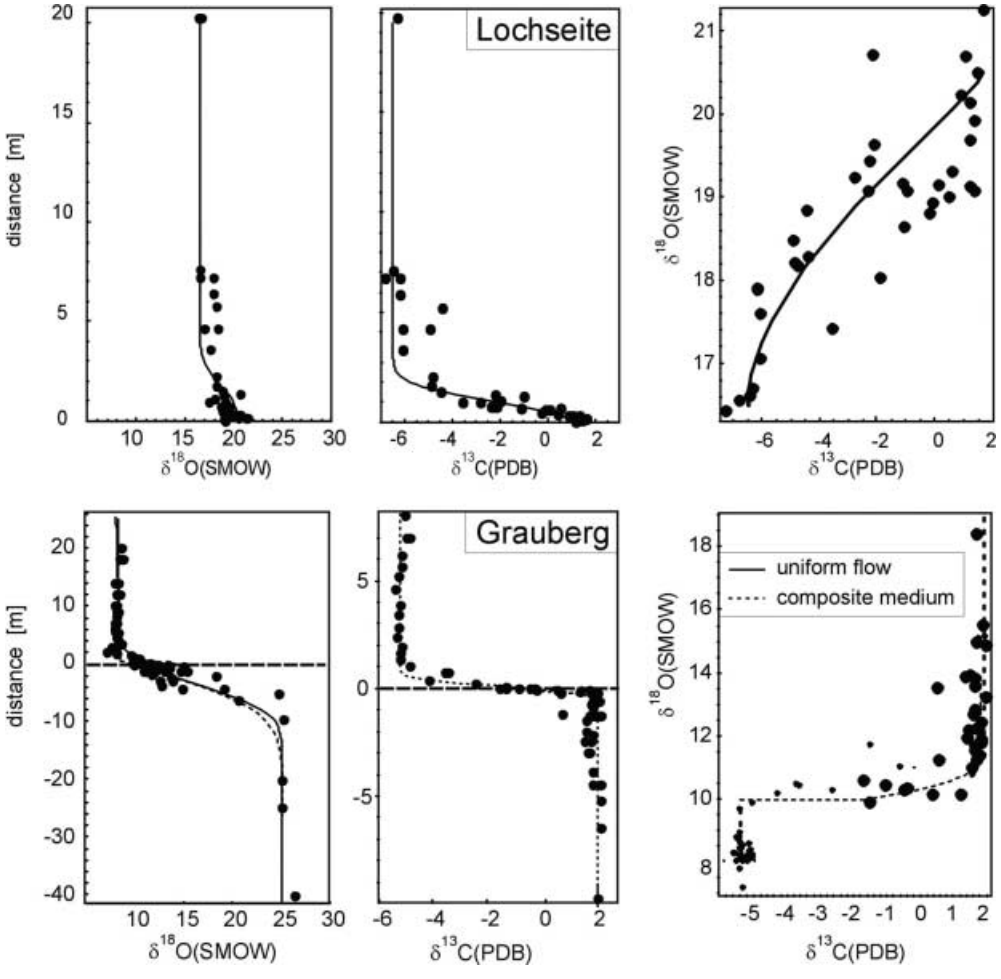


**Fig. 7a.** Model oxygen and carbon isotope fronts fitted to the data from the Lochseite locality assuming constant isotopic composition buffered by the pore fluid of the flysch at the thrust contact ('pinned boundary model' of Bickle and Baker 1990). **b** Model oxygen and carbon isotope fronts fitted to the data from the Grauberg locality; *solid line* uniform flow model; *dashed line* composite medium model, see text for the corresponding model assumptions

**Table 1.** Number of oxygen and carbon atoms per formula unit and molar volumes of the rock forming minerals and possible pore fluids; thermodynamic data taken from Holland and Powell (1998), fluid molar volumes calculated from the Kerrick and Jakobs (1981) fluid equation of state

| Mineral | Mineral | | | | | $H_2O$–$CO_2$ fluid[a] | | | | |
|---|---|---|---|---|---|---|---|---|---|---|
| | qtz | ab | mus | chl | cc | | | | | |
| $X_{CO2}$ | | | | | | 0 | 0.005 | 0.05 | 0.25 | 0.5 |
| Oxygen a.p.f.u. | 2 | 8 | 12 | 18 | 3 | 1 | 1.005 | 1.05 | 1.25 | 1.5 |
| Carbon a.p.f.u. | 0 | 0 | 0 | 0 | 1 | 0 | 0.005 | 0.05 | 0.25 | 0.5 |
| Molar volume ($cm^3$/mol) | 22.7 | 100.4 | 140.8 | 210.9 | 37.0 | 19 | 19 | 20 | 24 | 30 |

[a]For the calculation of the fluid molar volumes, conditions of 300 °C and 300–450 MPa were assumed

within this lithology. As a consequence, the isotopic composition at the calc-mylonite/Verrucano contact was largely buffered by the pore fluid of the flysch. In this situation, the initial and boundary conditions may be stated as:

$$\begin{aligned} R_f &= R_f^h \quad \text{at } t = 0 \quad \text{for } x > 0 \\ R_f &= R_f^h \quad \text{at } t = 0 \quad \text{at } x = 0 \end{aligned} \tag{2}$$

where $R_f^h$ is the isotopic composition of the pore fluid in equilibrium with the unaltered hanging wall Verrucano and $R_f^f$ is the isotopic composition of the fluid infiltrating from the footwall. Provided local isotopic equilibrium is maintained during alteration, the solution to Eq. (1) subject to the initial and boundary conditions in Eq. (2) is given by (e.g. Lapidus and Amundson 1952):

$$R_f(x,t) = R_f^h + 0.5\left(R_f^f - R_f^h\right)\left(1 + F(x,t) + e^{\frac{vx}{D}}G(x,t)\right) \quad , \tag{3}$$

with

$$\begin{aligned} F(x,t) &= erf\left(\tfrac{v\sqrt{t}}{2\sqrt{D}} - \tfrac{x}{2\sqrt{Dt}}\right) \\ G(x,t) &= erfc\left(\tfrac{v\sqrt{t}}{2\sqrt{D}} + \tfrac{x}{2\sqrt{Dt}}\right) \end{aligned} \tag{4}$$

The relevant transport parameters, namely $\sqrt{D \cdot t}$ and $(v \cdot t)$ that may explain the oxygen and carbon isotope pattern at the Lochseite locality, were obtained by minimizing the variance, $\sigma^2$, of the model predictions with respect to the observational data[4]

$$\sigma^2 = \sum_N \frac{\left(R^{obs} - R^{\mathrm{mod}}\right)^2}{N} \quad , \tag{5}$$

where $R^{obs}$ and $R^{mod}$ are the observed, and modelled isotopic compositions and the sum is over $N$ observations. The corresponding model curves are shown in Fig. 7. The transport parameters obtained are $\sqrt{(D^O \cdot t)} = 0.70$m and $v^O \cdot t = 1.63$ m for oxygen and $\sqrt{(D^C \cdot t)} = 0.53$m and $v^C \cdot t = 1.42$ m for carbon[5].

To obtain time-integrated volumetric fluxes, the retardation of the tracer front with respect to the physical infiltration front must be considered. Provided that local equilibrium is maintained, the retardation factor, $R_d$, may be expressed as (e.g. Abart and Pozzorini 2000):

$$R_d = \left(1 + \sum_{k=1}^{M} \frac{X_k}{X_f}\alpha_k\right) \quad , \tag{6}$$

where $\alpha_k$ is the equilibrium fractionation factor for isotopic exchange between mineral $k$ and the pore fluid. $R_d$ may be expressed as a function of the volumetric porosity $\phi$:

$$R_d = \left(1 + \frac{1-\phi}{\phi}\kappa\right) \quad , \tag{7}$$

with

$$\kappa = \frac{n^{\varepsilon}_{\mathrm{rock}}\bar{v}_{\mathrm{fluid}}}{n^{\varepsilon}_{\mathrm{fluid}}\bar{v}_{rock}} \cdot \alpha_k \tag{8}$$

and $n^{\varepsilon}_{\mathrm{rock}}$ and $n^{\varepsilon}_{\mathrm{fluid}}$ are the numbers of moles of the isotopic element $\epsilon$ per mole of rock and fluid and $\bar{v}_{rock}$ and $\bar{v}_{\mathrm{fluid}}$ are the corresponding molar volumes. For small porosities the retardation factor may be approximated by:

$$R_d \approx \frac{\kappa}{\phi} \quad . \tag{9}$$

The time-integrated volumetric fluid flux, TIFF is related to $(v \cdot t)$ by:

$$TIFF = (v \cdot t) \cdot \phi \tag{10}$$

Scaling for the retardation using Eq. (9) yields:

$$TIFF = (v \cdot t) \cdot \kappa \tag{11}$$

Because $\alpha_k$ is close to unity, $\kappa$ is merely a function of the fluid/solid partitioning of the isotopic element [see Eq. (8)]. The carbon and oxygen contents and molar volumes of the relevant rock forming minerals and

[4]$\sqrt{D \cdot t}$ has dimensions of length and is usually referred to as the characteristic length of diffusion.

[5]Upwards-directed flow has a positive downwards-directed flow has a negative sign.

possible pore fluids are given in Table 1. The fluid/solid partitioning estimated for the different rock types are given in Table 2.

The effective fluid/solid partitioning and the extent of retardation will be diminished if some minerals of a rock fail to react in exchange equilibrium with the pore fluid (e.g. Abart and Pozzorini 2000). Kinetically controlled mineral–fluid exchange is indicated by the systematics of the inter-mineral fractionations in the Verrucano from the Lochseite locality. At 220 °C, the quartz–calcite oxygen isotope fractionation is 2.06 (Matthews et al. 1983) to 3.87‰ (Chiba et al. 1989), depending on the calibration used. The fact that at Lochseite the quartz–calcite oxygen isotope fractionation is reversed at distances of more than about 1 m above the thrust indicates a departure from equilibrium. At Lochseite, the calcite–albite oxygen isotope fractionations vary between 3 and 6‰. They are generally larger than the calcite–albite equilibrium fractionation, which is predicted to be 1.14 (Zheng 1993) to 2.30‰ (Chiba et al. 1989) at 220 °C. At distances of more than 1 m above the thrust, calcite is too isotopically enriched to be in oxygen isotope equilibrium with quartz and albite. In the course of recrystallization during thrusting, calcite attained isotopic equilibrium with the local pore fluid. At distances of more than about 2 m above the thrust, oxygen isotope exchange between quartz and albite and the fluid was insignificant and quartz and albite preserved their original (pre-thrusting) oxygen isotope compositions. Only within the lowermost 1–2 m above the thrust they were both shifted to higher $^{18}O$ values. Textural forms, such as fibrous quartz in pressure fringes and as fracture fillings (see Fig. 2b, c), suggest that oxygen isotope exchange was facilitated by syntectonic stress-induced recrystallization within this zone of the Verrucano. However, these recrystallization effects quickly die out upwards after about 1 m. The effect of varying rates of mineral fluid exchange may be considered in a semi-quantitative way by accounting for the presence of slow exchanging phases in the calculation of the fluid–solid partitioning. In Table 2, the $\kappa^O$ factors for the Lochseite Verrucano are given for three different scenarios regarding the mineral–fluid exchange rates. In the local equilibrium scenario all minerals are regarded to be in oxygen isotope equilibrium with the pore fluid. Although not justified in light of the systematics of the inter-mineral fractionations, this scenario may be considered as a conservative maximum estimate of the $\kappa^O$ factors. In the inert quartz and albite scenario, all phases except for quartz and albite were assumed to be in exchange equilibrium with the local pore fluid. This is considered to be the most realistic scenario, because a

**Table 2.** $\kappa$ factors expressing the fluid/solid partitioning of oxygen and carbon for the different rock types and a variety of fluid compositions; the $\kappa$ factors enter the calculation of time integrated volumetric fluid fluxes from $v{\cdot}t$ estimates obtained from curve fitting

| Rock type[a] | $X_{CO2}$ | $\kappa^O$ | $\kappa^C$ |
|---|---|---|---|
| Footwall limestones from Grauberg | 0.000 | 1.54 | $\rightarrow\infty$ |
| Local equilibrium | 0.005 | 1.54 | 93.2 |
| | 0.050 | 1.55 | 9.8 |
| | 0.250 | 1.56 | 2.3 |
| | 0.500 | 1.62 | 1.5 |
| Verrucano, Grauberg | 0.000 | 1.56 | $\rightarrow\infty$ |
| Local equilibrium | 0.005 | 1.57 | 5.130 |
| | 0.050 | 1.60 | 0.540 |
| | 0.250 | 1.62 | 0.130 |
| | 0.500 | 1.69 | 0.008 |
| Verrucano, Grauberg | 0.000 | 1.17 | $\rightarrow\infty$ |
| Inert quartz | 0.005 | 1.17 | 5.130 |
| | 0.050 | 1.19 | 0.540 |
| | 0.250 | 1.20 | 0.130 |
| | 0.500 | 1.25 | 0.008 |
| Verrucano, Lochseite | 0.000 | 1.56 | $\rightarrow\infty$ |
| Local equilibrium | 0.005 | 1.57 | 5.130 |
| | 0.050 | 1.60 | 0.540 |
| | 0.250 | 1.62 | 0.130 |
| | 0.500 | 1.68 | 0.008 |
| Verrucano, Lochseite | 0.000 | 0.64 | $\rightarrow\infty$ |
| Inert quartz and albite | 0.005 | 0.64 | 5.130 |
| | 0.050 | 0.65 | 0.540 |
| | 0.250 | 0.65 | 0.130 |
| | 0.500 | 0.68 | 0.008 |
| Verrucano, Lochseite | 0.000 | 0.07 | $\rightarrow\infty$ |
| Only calcite reactive | 0.005 | 0.07 | 5.130 |
| | 0.050 | 0.08 | 0.540 |
| | 0.250 | 0.08 | 0.130 |
| | 0.500 | 0.08 | 0.008 |

[a]Modal proportions were taken as *footwall limestones* 95% calcite, 2.5% quartz, 2.5% muscovite; *Verrucano, Grauberg* 25% quartz, 25% albite, 25% muscovite, 20% chlorite, 5% calcite; *Verrucano, Lochseite* 30% quartz, 30% albite, 25% muscovite, 10% chlorite, 2.5% calcite

significant fraction of muscovite (illite) and chlorite was newly formed and calcite was remobilized during thrusting and most likely attained oxygen isotope equilibrium with the pore fluid. The only calcite reactive scenario treats all phases except for calcite as inert with respect to oxygen isotope exchange. This scenario yields minimum estimates for the $\kappa^O$ factors.

Considering the entire range of feasible fluid/solid oxygen partitioning, the corresponding $\kappa^O$ factors may vary from 0.08 to 1.60 at the Lochseite locality (see Table 2). The corresponding time-integrated upwards-directed volumetric fluid fluxes are 0.13–2.6 $m^3/m^2$. Given the fact that time-integrated fluid fluxes derived from the oxygen and carbon isotope fronts must be the same suggests that $\kappa^O/\kappa^C \approx \left(v^C \cdot t\right)/\left(v^O \cdot t\right) = 0.87$. For the local equilibrium scenario and for the quartz–albite inert scenario, this corresponds to fluid compositions with $0.005 < X_{CO2} < 0.05$, and the corresponding time-integrated volumetric flux is 1.0–2.6 $m^3/m^2$. The corrected $\sqrt{D \cdot t}$ parameters are 0.55–0.9 m for oxygen and 0.39–1.2 m for carbon.

## Oxygen and carbon isotope fronts at the Grauberg locality

At Grauberg, both the footwall and the hanging wall rocks are isotopically altered. A fixed concentration boundary condition, thus, is not applicable and mass transport must be modelled explicitly in both the Verrucano and in the footwall limestones. The initial and boundary conditions may be stated as:

$$\begin{aligned} &R_f = R_f^h \text{ for } x > 0, \quad R_f = R_f^f \text{ for } x < 0 \text{ at } t = 0 \\ &R_f = R_f^h \text{ for } x = \infty, \quad R_f = R_f^f \text{ for } x = -\infty \text{ at } t > 0 \end{aligned} \tag{12}$$

### *Uniform flow model*

One possibility to model material transport at Grauberg is to consider diffusion/dispersion and fluid advection across the thrust contact, and to treat effective diffusivities and fluid flow velocities as being uniform throughout the system (uniform flow model of Bickle and Baker 1990). For this model, Eq. (1) may be reduced to a pure diffusion equation by transforming the $x$-coordinate to account for the displacement of the tracer front by fluid advection. If the new space coordinate is taken as $(x + v{\cdot}t)$, the solution to Eq. (1) as subject to the initial and boundary conditions in Eq. (12) is given by (e.g. Crank 1975, Eq. 2.14):

$$R_f(x,t) = R_f^f + 0.5\left(R_f^f - R_f^h\right) \cdot erfc\left(\frac{x + vt}{2\sqrt{Dt}}\right) \tag{13}$$

The curves obtained from fitting this model to the isotope data from Grauberg are shown in Fig. 7. The transport parameters obtained are $\sqrt{\left(\mathrm{D^O} \cdot \mathrm{t}\right)} = 2.6\mathrm{m}$ and $v^O{\cdot}t = -3.8$ m for oxygen and $\sqrt{\left(\mathrm{D^C} \cdot \mathrm{t}\right)} = 0.17\mathrm{m}$ and $v^C{\cdot}t = 0.08$ m for carbon.

For the footwall carbonates, the fluid/solid partitioning was calculated assuming local isotopic equilibrium (see Table 2). Even if mineral–fluid oxygen isotope exchange may have been kinetically controlled for quartz and muscovite, this would only have a negligible effect on the fluid/solid partitioning because of the small amount of quartz and muscovite present. Burkhard et al. (1992) presented oxygen isotope data for albite, chlorite and muscovite from the hanging wall Verrucano at the Grauberg locality, which indicate that all phases except for quartz were in exchange equilibrium during thrusting. The quartz–calcite inter-mineral fractionations show a systematic decrease towards the thrust. This indicates that quartz–fluid oxygen isotope exchange was slow compared with the exchange of other minerals. This is why a local equilibrium and an inert quartz scenario are considered for Verrucano at Grauberg (see Table 2).

In the uniform flow model, the effective retarded diffusivities/dispersivities and effective retarded fluid-flow velocities are regarded as constant throughout the system. For a given fluid composition, the carbon fluid/solid partitioning is smaller in the footwall than in the hanging wall (see Table 2). Thus, the retardation of a carbon isotope front with respect to the physical infiltration front will be larger in the footwall than in the hanging wall.

This is incompatible with the model assumption of constant retarded effective diffusivities and retarded fluid-flow velocities as inherent in the uniform flow model. Therefore, only the oxygen isotope front may be interpreted in the framework of this model.

Regardless of the fluid composition, the $\kappa^O$ factor is about 1.6 and the downward-directed time-integrated fluid flux is estimated at 6.1 $m^3/m^2$. The corresponding corrected $\sqrt{\left(\mathrm{D^O} \cdot \mathrm{t}\right)}$ parameter is 3.3 m.

## Diffusion/dispersion in a composite system

In an alternative model, the fronts at Grauberg may be interpreted as being caused by diffusive/dispersive isotope exchange between the footwall and hanging wall, whereby the effective diffusivities/dispersivities are considered to be different in the two lithologies. For the initial and boundary conditions stated in Eq. (12) the solution for this model is given by (e.g. Crank 1975):

$$\begin{aligned} R_f^h(x,t) &= \frac{1}{1 + \sqrt{D_f/D_h}} \\ &\quad \times \left(1 + \sqrt{D_f/D_h} + erf\left(\frac{x}{2\sqrt{D_h t}}\right)\right) \text{ footwall} \\ R_f^f(x,t) &= \frac{1}{1 + \sqrt{D_f/D_h}}\, erfc\left(\frac{|x|}{2\sqrt{D_f t}}\right) \text{ hangingwall} \end{aligned} \tag{14}$$

$D_f$ and $D_h$ are the effective diffusivities/dispersivities in the footwall and hanging wall, respectively. The

corresponding model curves are shown in Fig. 7. The transport parameters obtained are $\sqrt{(D_h^O \cdot t)} = 45.6\,m$ and $\sqrt{(D_f^O \cdot t)} = 4.1\,m$ for oxygen and $\sqrt{(D_h^C \cdot t)} = 0.14\,m$ and $\sqrt{(D_f^C \cdot t)} = 0.1\,m$. The $\sqrt{(D^O \cdot t)}$ parameters corrected for the fluid/solid oxygen partitioning are 5.2 m for oxygen diffusion/dispersion in the footwall carbonates and 50–57.6 m for oxygen diffusion/dispersion in the hanging wall Verrucano. Given that the effective diffusivity is on the same order of magnitude for carbon- and oxygen-bearing species in an aqueous fluid, the $\sqrt{(D \cdot t)}$ parameters obtained from the oxygen and carbon fronts should be comparable. For the footwall carbonates, the relation $\kappa^O/\kappa^C \approx (D^C \cdot t)/(D^O \cdot t) = 1/1720$ indicates very low carbon contents of the infiltrating fluid with $0 < X_{CO2} < 0.005$ (see Table 2). The corrected $\sqrt{(D^C \cdot t)}$ parameter is hence $> 0.96$ m in the footwall and, provided that $X_{CO2}$ was uniform throughout the system, $\sqrt{(D^C \cdot t)} > 0.3\,m$ in the hanging wall. Even if no advection in the direction perpendicular to the thrust contact is allowed in this model, it indicates that material transport was significantly more efficient in the hanging wall Verrucano than in the footwall limestones. The hanging wall Verrucano again probably acted as a source of isotopically light oxygen that caused alteration of the footwall limestone.

## Effective diffusivities/dispersivities

Effective oxygen diffusivities calculated from $\sqrt{D^O \cdot t}$ for geologically meaningful time scales are given in Table 3. The effective diffusivity of a species in the pore fluid of a porous medium is related to the diffusivity of the same species in the free fluid, $D_0$, by:

$$D = \tau \phi D_0 \quad (15)$$

where $\tau$ is the tortuosity of the porous medium. The experimentally determined diffusivity of the $H_2O$ species in water is about $5\times10^{-8}$ $m^2/s$ at 250 °C (Franck et al. 1996). In geological materials the porosity may vary considerably from about $10^{-4}$ to $10^{-2}$. The tortuosity may vary between 0.1 and $\leq 1$. If $\phi$ were $10^{-2}$ and $\tau$ were 0.1, an effective diffusivity of $5\times10^{-11}$ $m^2/s$, and if $\phi$ were $10^{-4}$ and $\tau$ were 0.1, an effective diffusivity of $7.3\times10^{-13}$ $m^2/s$ would be calculated from the experimental data. Comparison with the values obtained from curve fitting (see Table 3) shows that molecular diffusion of $H_2O$ in the pore fluid may well explain the inferred diffusive/dispersive contribution to oxygen transport at the Lochseite and Grauberg localities, even for the short-term scenario. Only the rate of diffusion/dispersion as derived from the composite medium model for the hanging wall Verrucano at Grauberg is too fast to be explained by molecular diffusion of $H_2O$ in the pore fluid.

In this case, the contribution of hydrodynamic dispersion may explain the enhancement of diffusion/dispersion. Because there is no advective flow component allowed in the direction perpendicular to the thrust surface in this model, this is interpreted as transversal dispersion associated with thrust parallel flow.

## Strontium isotope variations

The Sr-isotope profiles from the Grauberg and Lochseite localities qualitatively show the same features as the carbon and oxygen isotope patterns. At both localities, the $^{87}Sr/^{86}Sr$ ratios show a monotonic enrichment/depletion trend across the thrust. No local $^{87}Sr/^{86}Sr$ minima/maxima at the thrust surface that testify to the introduction of externally derived strontium by flow along the thrust could be identified. The observed patterns may be explained by strontium exchange between the more radiogenic strontium reservoir of the hanging wall and the less radiogenic strontium reservoir of the footwall lithologies. The major difference between the two profiles is that at Grauberg most of the alteration occurs below the thrust contact, whereas at Lochseite most of the alteration occurs in the hanging wall.

The fact that at Grauberg the Sr-isotope values at the thrust contact (0.714) are closer to the presumed background values of the Verrucano (0.7136–0.7211; Hunziker et al. 1986) than to the presumed background composition of the footwall carbonates (0.707–0.7089;

**Table 3.** Effective oxygen diffusivities/dispersivities in $m^2/s$ calculated from $\sqrt{(D^O \cdot t)}$ as obtained from curve fitting

| | Lochseite | | Grauberg | | | |
|---|---|---|---|---|---|---|
| | Pinned boundary model | | Uniform flow model | Composite medium model | | |
| | min. | max. | | Footwall | Hanging wall | |
| | | | | | min. | max. |
| $\sqrt{(D^O \cdot t)}$ (m) | 0.55 | 0.9 | 3.3 | 5.2 | 50 | 57.6 |
| time (years) | | | | | | |
| $10^5$ | $9.5\times10^{-14}$ | $2.5\times10^{-13}$ | $3.4\times10^{-12}$ | $8.7\times10^{-12}$ | $7.9\times10^{-10}$ | $1.1\times10^{-9}$ |
| $10^6$ | $9.5\times10^{-15}$ | $2.5\times10^{-14}$ | $3.4\times10^{-13}$ | $8.7\times10^{-13}$ | $7.9\times10^{-11}$ | $1.1\times10^{-10}$ |
| $10^7$ | $9.5\times10^{-16}$ | $2.5\times10^{-15}$ | $3.4\times10^{-14}$ | $8.7\times10^{-14}$ | $7.9\times10^{-12}$ | $1.1\times10^{-11}$ |

DePaolo 1986; Burke et al. 1982), and that the strontium isotope alteration is more pronounced in the footwall limestones, suggests a net strontium transfer from the hanging wall to the footwall.

At Lochseite, the strontium isotope values at the calc-mylonite/Verrucano contact (0.710) are closer to the presumed 'background' compositions of the footwall flysch (0.7089–0.713; Hunziker et al. 1986) than to the presumed strontium isotope compositions of the Verrucano, and strontium isotope alteration is essentially confined to the hanging wall. This indicates an upwards-directed strontium transfer across the thrust. The fact that the Lochseiten calc-mylonite is practically identical to the flysch with respect to its $^{87}Sr/^{86}Sr$ ratios is compatible with a derivation of its carbonate matrix from the footwall flysch. The veined nature of the calc-mylonite and its relatively constant $^{87}Sr/^{86}Sr$ ratios (0.7096–0.7103; Burkhard et al. 1992) suggest precipitation from a flysch-derived strontium-bearing fluid.

## Fluid regimes at the Glarus thrust

A qualitative model of the regional flow pattern associated with the active Glarus thrust is illustrated in Fig. 8. Mineralogical alteration, such as the carbonatization of the lowermost 10–20 cm of the hanging wall Verrucano and the partial dolomitization of the uppermost footwall limestones at Grauberg, as well as the oxygen, carbon and strontium isotope patterns in the two vertical profiles at the Grauberg and Lochseite localities, give unambiguous evidence of material transport across the thrust. With respect to the vertical transport components, the southern section of the Glarus thrust, where the footwall is represented by Mesozoic limestones, behaved fundamentally differently from the northern section, where the footwall is represented by Tertiary flysch. Both the uniform flow model and the composite medium model suggest that, at the Grauberg locality in the south, net mass transport was from the hanging wall Verrucano into the footwall limestones. In contrast, the front geometries at the Lochseite locality in the north indicate net transport from the footwall flysch into the hanging wall Verrucano. As a consequence, the oxygen isotope composition at the calc-mylonite/Verrucano contact and, in particular, the composition of the Lochseiten calc-mylonite, was buffered towards the Verrucano composition in the south and towards the flysch composition in the north (see inserts in Fig. 8). The position of the regional scale oxygen isotope front postulated by Burkhard and Kerrich (1990), Bowman et al. (1994) and more recently by Badertscher et al. (2002) for along-thrust flow approximately coincides with the lithological boundary between Mesozoic limestone and Tertiary flysch in the footwall of the thrust (Fig. 1b). In the light of the vertical transport components shown by the cross thrust oxygen, carbon and strontium isotope profiles we suggest that the regional south to north $^{18}O$ enrichment trend was simulated by cross thrust transport.

At the Lochseite locality, the water required for the observed hydration of the lowermost Verrucano may be locally derived from the underlying flysch. This is corroborated by upwards-directed flow as inferred from the stable and strontium isotope patterns at Lochseite. Dewatering of the flysch during regional low-grade metamorphism involving the illite to muscovite transition and compaction during thrusting are likely scenarios that may explain upwards migration of flysch-derived fluids. In contrast, at the Grauberg locality there is no obvious local water source nor any isotopic indication for upwards-directed flow. There the water required for the observed hydration of the bottom of the Verrucano was probably introduced by flow along the thrust. If externally derived fluids indeed migrated along the thrust, then the contrasting effective oxygen diffusivities/dispersivities in the footwall and hanging wall derived from the composite medium model indicate that thrust parallel flow primarily occurred within the Verrucano. A minimum estimate for the horizontal flow

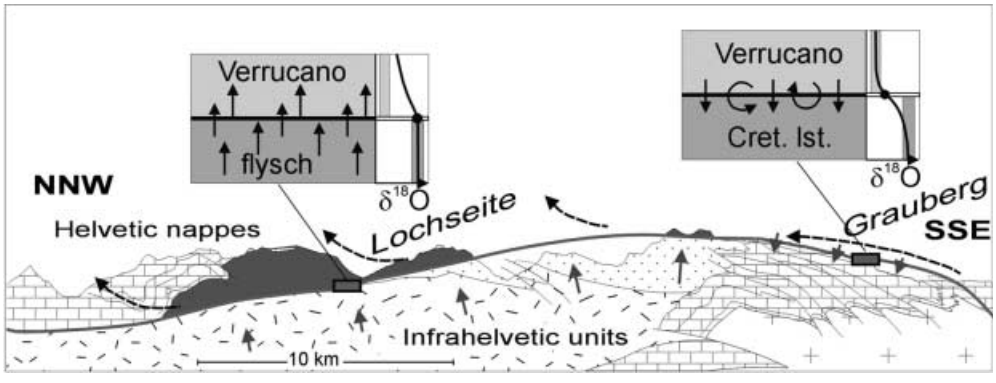


**Fig. 8.** Qualitative model of syndeformative fluid flow along the Glarus thrust; *small downwards pointing solid arrows* at the southern section of the thrust represent lateral dispersion and seepage associated with subhorizontal flow in the Verrucano aquifer into the footwall; *upwards directed solid arrows* in the footwall of the northern section indicate upwards fluid migration because of dewatering and compaction of the N-Helvetic flysch; *dashed arrows* indicate the supposed regional flow pattern; *insets* illustrate the effect of vertical transport components on the oxygen isotope composition of the Lochseiten calc-mylonite

component may be derived from the fact that the bulk rock water content of Verrucano increased by about 2 wt% (see Fig. 3).

Given that the density of Verrucano is approximately 2,700 kg/m$^3$, this corresponds to an introduction of about 54 kg or 0.06 m$^3$ $H_2O$ per m$^3$ of rock. In a south to north cross section, the portion of the Glarus thrust with Mesozoic limestone in the footwall is exposed over a distance of about 4 km. Based on the assumption that the hydration of the Verrucano occurred at local fluid–rock equilibrium and that it is exclusively because of the northwards migration of aqueous fluids along the thrust, a horizontal flux on the order of 240 m$^3$/m$^2$ is derived.[6]

The isotopic alteration of the footwall in the southern section of the thrust may be interpreted as lateral fronts that developed by diffusive/dispersive exchange between footwall and hanging wall, and possibly by a small vertical flow component caused by lateral seepage from the Verrucano aquifer into the relatively less permeable footwall limestones. Pronounced small-scale oxygen isotope variations in the footwall limestones (see Fig. 5) indicate a heterogeneous permeability structure. Transport along discrete high permeability structures contributed to transversal hydrodynamic dispersion. The isotopic and chemical alteration of the lowermost Verrucano at Grauberg are interpreted as a result of such transversal dispersion. Because of the low $X_{CO2}$ of the pore fluid, carbon isotope alteration is restricted to the uppermost 50 cm of the footwall limestones.

In the north, where the footwall is represented by Tertiary flysch, along thrust flow was probably deflected upwards by fluids ascending from the flysch. The Verrucano appears to have been less permeable to upwards-directed flow than the footwall lithologies. Ascending fluids in the flysch were ponded below the Verrucano, leading to near lithostatic fluid pressures at the thrust. This provoked brittle failure, minimized normal stress and facilitated motion along the thrust (Price 1988).

The Lochseiten calc-mylonite has been interpreted as an extremely smeared out Infrahelvetic limestone (Schmid 1975). Alternatively, it has been regarded as a secondary mineralization of the thrust surface (Rothpletz 1883; Burkhard and Kerrich 1990). At the Lochseiten locality, the Lochseiten calc-mylonite is characterized by an extremely high density of calcite veins, and it is in carbon, oxygen and strontium isotope equilibrium with the underlying flysch.

Therefore, at Lochseite, we concur with a significant contribution to the carbonate content of the Lochseiten calc-mylonite by secondary hydrothermal calcite precipitation. The carbonate was probably introduced into the thrust surface via the pore fluid migrating upwards from the calcite-saturated footwall flysch. The solubility of calcite was probably controlled by the reaction:

$$CaCO_3 + CO_2 + H_2O = Ca^{2+} + 2HCO_3^-$$

In a low salinity aqueous solution the solubility of calcite decreases with decreasing $CO_2$ partial pressure and with increasing temperature (e.g. Rimstidt 1997). An increase in metamorphic grade from the footwall to the hanging wall has been documented by Frey (1988). A sharp temperature step at the thrust surface is, however, unlikely. The pronounced localization of calcite vein formation within the thrust plane is probably caused by syntectonic pressure perturbations. Thrusting probably occurred by an alternation of brittle and ductile mechanisms (Badertscher and Burkhard 2001). Fracturing that occurred in episodes of relatively high, close to lithostatic fluid pressure may have caused short-term pore-pressure reductions. During such events $CO_2$ may have unmixed from the pore fluid leaving behind an aqueous solution that was supersaturated with respect to calcite. Subsequent calcite precipitation in veins and fractures gave the Lochseiten calc-mylonite its veined nature.

## Summary and conclusions

The $^{18}O$, $^{13}C$ and $^{87}Sr/^{86}Sr$ variations along two vertical profiles across the Glarus thrust at Grauberg in the south and at Lochseiten in the north reveal fundamentally different flow regimes during deformation. In the southern section of the thrust, where the footwall is represented by Mesozoic limestones, net material transport across the thrust was directed downwards. In the northern section of the thrust, where the footwall is represented by Tertiary flysch, net material transport across the thrust was directed upwards. In the southern section of the thrust, a horizontal flow component is inferred from the hydration of the lowermost 10–20 m of the hanging wall Verrucano. In the south, horizontal flow mainly occurred within the Verrucano, and the isotopic alteration of the footwall carbonates is ascribed to transversal hydrodynamic dispersion associated with horizontal flow and/or to lateral seepage from the Verrucano aquifer into the footwall lithologies. If at all present in the north, horizontal flow was deflected upwards by fluids ascending from the dewatering and compacting flysch. Even if the vertical components of flow were at least two orders of magnitude smaller than horizontal flow, material transport across the thrust was sufficient to largely control the $^{18}O$ signature of the Lochseiten calc-mylonite. The apparent one-dimensional front geometry of the regional south to north $^{18}O$-enrichment trend in the Lochseiten calc-mylonite may largely be explained by the differences in the vertical flow components in the southern and northern sections of the thrust. In the south, downwards-directed material transfer led to the imprint of the Verrucano isotopic signature on the Lochseiten calc-mylonite. In the north,

[6]This estimate is about one order of magnitude lower than integrated fluxes derived from the regional south to north $^{18}O$ enrichment trend of calcites from the Lochseiten mylonite described by Bowman et al. (1994) and by Badertscher et al. (2002).

upwards-directed material transfer led to the imprint of the flysch isotopic signature on the Lochseiten calc-mylonite. In the south, the calc-mylonite at the thrust surface is largely derived from the underlying Mesozoic carbonates; only a small fraction is represented by secondary calcite precipitates. In the north, the Lochseiten calc-mylonite supposedly has obtained a significant fraction of its carbonate content by precipitation of calcite from ascending fluids in chemical and isotopic equilibrium with the footwall flysch.

**Acknowledgements** This manuscript greatly benefited from perceptive reviews by P. Blattner, A. Skelton and S. Schmid. We want to thank H. Eppel and T. Widmer for their help in field and laboratory work. Financial support by the Austrian National Bank Jubiläumsfonds grant 7133 is gratefully acknowledged.

## References

Abart R, Pozzorini D (2000) Implications of kinetically controlled mineral–fluid exchange on the geometry of stable isotope fronts. Eur J Mineral 12:1069–1082

Arkai P, Balogh K, Frey M (1997) The effects of tectonic strain on crystallinity, apparent mean crystallite size and lattice strain of phyllosilicates in low-temperature metamorphic rocks. A case study from the Glarus overthrust, Switzerland. Schweiz Mineral Petrogr Mitt 77:27–40

Badertscher N, Burkhard M (2001) Brittle–ductile deformation in the Glarus thrust Lochseiten (LK) calc-mylonite. Terra Nova 12:281–288

Badertscher N, Abart R, Burkhard M (2002) The role of fluids in thrusting of the Helvetic Glarus overthrust (in review)

Baumgartner L, Rumble D (1988) Transport of stable isotopes: I: development of a kinetic continuum theory for stable isotope transport. Contrib Mineral Petrol 98:417–430

Bear J (1972) Dynamics of fluids in porous media. Elsevier, Amsterdam

Bickle M, Baker J (1990) Advective–diffusive transport of isotopic fronts: an example from Naxos, Greece. Earth Planet Sci Lett 97:78–93

Bickle M, McKenzie D (1987) The transport of heat and matter by fluids during metamorphism. Contrib Mineral Petrol 95:384–392

Bowman JR, Willett SD, Cook SJ (1994) Oxygen isotopic transport and exchange during fluid flow: one-dimensional models and applications. Am J Sci 294:1–55

Burke WH, Denison RE, Hetherington EA, Koepnik RB, Nelson HF, Otto JB (1982) Variation of seawater $^{87}Sr/^{86}Sr$ throughout Phanerozoic time. Geology 10:516–519

Burkhard M, Kerrich R (1990) Fluid–rock interactions during thrusting of the Glarus nappe – evidence from geochemical and stable isotope data. Schweiz Mineral Petrogr Mitt 70:77–82

Burkhard M, Kerrich R, Fyfe WS (1992) Stable and Sr-isotope evidence for fluid advection during thrusting of the Glarus nappe (Swiss Alps). Contrib Mineral Petrol 112:293–311

Chiba H, Chacko T, Clayton RN, Goldsmith JR (1989) Oxygen isotope fractionations involving diopside, forsterite, magnetite and calcite: application to geothermometry. Geochim Cosmochim Acta 53:2985–2995

Cox SF, Etheridge MA, Wall VI (1986) The role of fluids in syntectonic mass transport, and the localization of metamorphic vein-type ore deposits. Ore Geol Rev 2:63–86

Crank J (1975) The mathematics of diffusion. Oxford, Clarendon press

DePaolo DJ (1986) Detailed report of the Neogene Sr isotopic evolution of seawater from DSDP site 590b. Geology 14:103–106

Etheridge MA, Wall VJ, Vernon RH (1984) The role of the fluid phase during regional metamorphism and deformation. J Metamorph Geol 1:205–226

Franck EU, Wiegand G, Dalmen N (1996) Water. In: Ullmann's encycopedia of industrial chemistry, 28A. Verlag Chemie, Weinheim

Frey M (1988) Discontinuous inverse metamorphic zonation, Glarus Alps, Switzerland: evidence from illite crystallinity data. Scweiz Mineral Petrogr Mitt 68:171–184

Funk HP, Labhart T, Milnes AG, Pfiffner OA, Schaltegger U, Schindler C, Schmid SM, Trümpy R (1983) Bericht über die Jubil\äumsexkursion Mechanismus der Gebirgsbildung der Schweizerischen Geologischen Gesellschaft in das ost- und zentralschweizerische Helvetikum und in das nördliche Aaremassiv vom 12. bis 17 September 1982. Eclogae Geol Helv 76:91-123

Fyfe WS, Kerrich R (1985) Fluids and thrusting. Chem Geol 49:353–362

Fyfe WS, Price NJ, Thompson AB (1978) Fluids in the Earth's crust. Elsevier, Amsterdam

Heim A (1921) Geologie der Schweiz, Bd. II. Tauchniz, Leipzig

Holland TJB, Powell R (1998) An internally consistent thermodynamic dataset for phases of petrologic interest. J Metamorph Geol 16:309–343

Hunziker JC (1987) Radiogenic isotopes in very low grade metamorphism. In: Frey M (ed) Low grade metamorphism. Blackie, Glasgow, pp 200–226

Hunziker JC, Frey M, Clauer N, Dallmeyer RD, Friedrichsen H, Flehmig W, Hochstrasser K, Roggwiler P, Schwander H (1986) The evolution of illite to muscovite: mineralogical and isotopic data from the Glarus Alps, Switzerland. Contrib Mineral Petrol 92:157–180

Kerrick DM, Jacobs GK (1981) A modified Redlich–Kwong equation for $H_2O$–$CO_2$ mixtures at elevated pressures and temperatures. Am J Sci 281:735–767

Kiely PV, Jackson ML (1964) Selective dissolution of micas from potassium feldspars by sodium pyrosulfate fusion of soils and sediments. Am Mineral 49:1648–1659

Lapidus L, Amundson NR (1952) Mathematics of adsorption in beds. IV. The effect of longitudinal diffusion in ion exchange and chromatographic columns. J Phys Chem 56:984–998

Matthews A, Goldsmith JR, Clayton RN (1983) Oxygen isotope fractionation involving pyroxenes: the calibration of mineral-pair geothermometers. Geochim Cosmochim Acta 47: 631–644

McCaig AM (1989) Fluid flow through fault zones. Nature 340:600

Milnes AG, Pfiffner OA (1980) Tectonic evolution of the central Alps in the cross section St. Gallen Como. Eclogae Geol Helv 73:619–633

Nabelek PL (1991) Stable isotope monitors. In: Kerrick DM (ed) Contact metamorphism. Rev Mineral 26:395–435

Oliver J (1986) Fluids expelled tectonically from orogenic belts, their role in hydrocarbon migration and other geologic phenomena. Geology 14:99–102

Pfiffner OA (1977): Tektonische Untersuchungen im Infrahelvetikum der Ostschweiz. Mitt Geol Inst ETH u\Univ Zürich N.F., 217

Pfiffner OA (1985) Displacements along thrust faults. Eclogae Geol Helv 78:313–333

Price RA (1988) The mechanical paradox of large overthrusts. Geol Soc Am Bull 100:1898–1908

Rahn M, Mullis J, Erdelbrock K, Frey M (1995) Alpine metamorphism in the North Helvetic Flysch of the Glarus Alps, Switzerland. Eclog Geol Helv 88:157–178

Rimstidt JD (1997) Gangue mineral transport and deposition. In: Barnes HL (ed) Geochemistry of hydrothermal ore deposits. Wiley, New York, pp 487–516

Rothpletz A (1883) Der Gebirgsbau der Alpen beiderseits des Rheins. Z Dtsch Geol Ges 167–168

Schmid SM (1975) The Glarus overthrust: field evidence and mechanical model. Eclogae Geol Helv 68:247–283

Schmid SM, Pfiffner OA, Froitzheim N, Schonborn G, Kissling E (1996) Geophysical–geological transect and tectonic evolution of the Swiss–Italian Alps. Tectonics 15:1036–1064

Sharp ZD (1990) In situ laser microprobe techniques for stable isotope analysis. Chem Geol 101:3–19

Sibson RH (1986) Earthquakes and rock deformation in crustal fault zones. Annu Rev Earth Planet Sci 14:149–175

Syers JK, Chapman SL, Jackson ML (1968) Quartz isolation from rocks, sediments and soils for determination of oxygen isotopes composition. Geochim Cosmochim Acta 32:1022–1025

Valley JW, Kitchen N, Kohn MJ, Niendorf CR, Spicuzza MJ (1995) UWG-2, a garnet standard for oxygen isotope ratios: strategies for high precision and accuracy with laser heating. Geochim Cosmochim Acta 59:5223–5231

Zheng YF (1993) Calculation of oxygen isotope fractionations in anhydrous silicate minerals. Geochim Cosmochim Acta 57: 1079–1091